Pharmaceutical Research, Vol. 27, No. 1, January 2010 (© 2009)
DOI: 10.1007/s11095-009-9992-1

Research Paper

PEGylated PAMAM Dendrimer-Doxorubicin Conjugates: *In Vitro* Evaluation and *In Vivo* Tumor Accumulation

Saijie Zhu,[1] Minghuang Hong,[1] Lihong Zhang,[1] Guotao Tang,[1] Yanyan Jiang,[1,2] and Yuanying Pei[1]

Received July 27, 2009; accepted September 30, 2009; published online October 28, 2009

Purpose. To investigate the effects of PEGylation degree and drug conjugation style on the *in vitro* and *in vivo* behavior of PEGylated polyamidoamine (PAMAM) dendrimers-based drug delivery system.
Methods. Doxorubicin (DOX) was conjugated to differently PEGylated PAMAM dendrimers by acid-sensitive *cis*-aconityl linkage and acid-insensitive succinic linkage to produce the products of PPCD and PPSD conjugates, respectively. *In vitro* evaluations including pH-dependent DOX release, cytotoxicity, cellular uptake, cell internalization mechanism, and intracellular localization were performed. Tumor accumulation was also visualized by *in vivo* fluorescence imaging.
Results. DOX release from PPCD conjugates followed an acid-triggered manner and increased with increasing PEGylation degree. *In vitro* cytotoxicity of PPCD conjugates against ovarian cancer (SKOV-3) cells increased, while cellular uptake decreased with increasing PEGylation degree. PPSD conjugates released negligible drug at any tested pH condition and were less cytotoxic. The conjugates were internalized by SKOV-3 cells via clathrin-mediated and adsorptive endocytosis, and were delivered to acidic lysosomes where DOX was released from PPCD conjugates and diffused into the nuclei. PPCD conjugates with highest PEGylation degree showed the highest tumor accumulation in mice inoculated with SKOV-3 cells.
Conclusion. The obtained results suggested that PPCD conjugates with highest PEGylation degree would be a potential candidate for solid tumor treatment.

KEY WORDS: acid-sensitive linkage; cellular uptake; doxorubicin; poly(amidoamine) dendrimer; poly (ethylene glycol).

INTRODUCTION

Drug-polymer conjugates are potential candidates for the selective delivery of anticancer agents to tumor tissue. The main advantages of conjugating drugs to polymeric carriers include (1) an increase in water solubility of low soluble or insoluble drugs, and therefore, enhancement of drug bioavailability, (2) protection of drug from deactivation and preservation of its activity during circulation, (3) a reduction in antigenic activity of the drug leading to a less pronounced immunological body response, and (4) the ability to provide passive or active targeting of the drug specifically to the site of its action (1).

Poly(amidoamine) (PAMAM) dendrimers are highly branched, narrowly dispersed synthetic macromolecules with well-defined structure and composition. The terminal amine groups of PAMAM dendrimers can be modified with different functionalities and can be linked with various biomolecules (2). These unique structural features of PAMAM dendrimers make them ideal nanoplatforms to conjugate biologically important substances (e.g., drugs, targeting molecules, and imaging agents) (3–5). However, it has been demonstrated that PAMAM dendrimers exhibit generation-dependent cytotoxicity (6). Polyethylene glycol (PEG) is a non-immunogenic, non-antigenic, non-toxic, highly water-soluble polymer. Modification of the amine groups of PAMAM dendrimers with PEG reduces the cytotoxicity and improves their biocompatibility (7). Besides, PEGylation improves the solubility of both drug and carrier system, minimizes aggregation of particulates and decreases the opsonization by reticuloendothelial system (RES) (8).

Incorporating acid-sensitive linkage between drugs and polymeric carriers is an attractive approach which ensures effective release of the polymer-bound drug at the tumor site, while keeping the conjugates stable in the bloodstream. The acid-triggered release occurred either in extracellular fluid, resulting from the slightly acidic condition in tumor tissue, or within tumor cells, in acidic lysosomes/endosomes after cellular uptake of drug-polymer conjugates (9). *Cis*-aconitic anhydride was first proposed by Shen and Ryser (10). Much of the literature has used this linkage to conjugate small molecular anticancer drugs to polymeric carriers to achieve acid-sensitive drug release and has confirmed its feasibility in controlling drug release. These polymeric carriers included

Electronic supplementary material The online version of this article (doi:10.1007/s11095-009-9992-1) contains supplementary material, which is available to authorized users.

[1] Department of Pharmaceutics, School of Pharmacy, Fudan University, 826 Zhangheng Road, Shanghai 201203, China.
[2] To whom correspondence should be addressed. (e-mail: yanyanjiang@shmu.edu.cn)

poly-D-lysine (10), *N*-(2-hydroxypropyl)methacrylamide (HPMA) (11), polyvinyl alcohol (PVA) (12), PLLA-PEG diblock copolymer (13), etc.

In the present study, doxorubicin (DOX), a widely used anticancer drug, was attached to the surface of PAMAM dendrimer with different PEGylation degrees via a pH-sensitive or pH-insensitive spacer. The effect of PEGylation degree and linkage style on the *in vitro* release, cytotoxicity against SKOV-3 cells and cellular uptake were investigated. The internalization mechanism of the DOX-polymer conjugates in SKOV-3 cells was studied in the presence of endocytosis inhibitors. The intracellular localization of the conjugates was visualized by confocal laser scanning microscopy. *In vivo* fluorescence imaging was also performed to evaluate the effect of PEGylation degree on the tumor-targeting characteristics of the PPCD conjugates in SKOV-3 tumor-bearing mice.

MATERIALS AND METHODS

Materials

PAMAM dendrimer generation 4 with an ethylenediamine core in methanol (10% *w*/*v*) was obtained from Dendritech, Inc. (Midland, MI, USA). Methoxy PEG Succinimidyl Carboxymethyl Ester with molecular weight of 5000 (MeO-PEG-SCM) was purchased from JenKem Technology Co., Ltd. (Beijing, China). *Cis*-aconitic anhydride was obtained from Alfa Aesar (Lancashire, UK). Anhydrous DMF, trypan blue, *p*-dioxane, succinic anhydride and sucrose were purchased from Sinopharm Chemical Reagent Co., Ltd. (Shanghai, China). 3-(4,5-dimethylthiazol-2-yl)-2,5-diphenyl tetrazolium bromide (MTT) was obtained from Amresco (Solon, OH, USA). 1-ethyl-3-(3-dimethylaminopropyl) carbodiimide hydrochloride (EDC) was purchased from Shanghai Medpep Co., Ltd. (Shanghai, China). Doxorubicin Hydrochloride (DOX) was from Zhejiang Hisun Pharmaceutical Co., Ltd. (Zhejiang, China). Sodium azide was kindly provided by the Department of Medicinal Chemistry, School of Pharmacy, Fudan University. 2-deoxy-d-glucose was purchased from Shanghai Jingchun Reagent Co., Ltd. (Shanghai, China). Filipin, Colchicine and Poly-L-lysine (M.W. 30000–70000) was from Sigma-Aldrich (Saint Louis, MO, USA). Hoechst 33342 was purchased from Beijing Solarbio Science & Technology Co., Ltd. (Beijing, China). Lysotracker Green DND-26 was obtained from Molecular Probes (Eugene, OR, USA). Chloroquine diphosphate was purchased from J&K Chemical Ltd. (Beijing, China).

Synthesis of PEG-PAMAM Conjugates with Different PEGylation Degrees

The condensation reaction between PAMAM dendrimer and PEG was carried out according to the method previously reported (8) with minor modification. The starting materials were G4 PAMAM dendrimer (64 amino groups, M.W. = 14 215) and MeO-PEG-SCM (M.W. = 4834 by MALDI-TOF MS). Three different PEG-PAMAM conjugates were synthesized as follows. Various amounts of PEG were added to the solution of PAMAM dendrimer (3.13 μmol, 44.4 mg) in 5 ml of 0.2 M phosphate buffer (pH 8.0), with molar ratio between PEG and PAMAM dendrimer of 4:1, 16:1 and 32:1. The reaction mixtures were incubated at room temperature for 24 h with stirring, placed in an ultrafiltration tube (Amicon Ultra-4, MWCO 30,000 for PEG-PAMAM 4/1; MWCO 50,000 for PEG-PAMAM 16/1 and 32/1) and centrifuged at 5,000 rpm for 25 min for 5–6 times. Thin layer chromatography (TLC) was used to monitor the purity of the products until no PEG could be detected in the upper solution (chloroform/methanol/water = 1/1/0.1, *v*/*v*/*v*) (PEG, Rf = 0.78). The products were retrieved by freeze drying from the aqueous solution, and white solids were obtained. The yields of PEG-PAMAM 4/1, 16/1 and 32/1 were 90.7%, 54.1% and 62.5%, respectively.

^{1}H-NMR spectra of synthesized PEG-PAMAM conjugates were recorded on a Mercury Plus 400 MHz spectrometer (Bruker, Germany). The PEGylation degree was estimated using the proton integration method, by taking the characteristic peaks of PEG and PAMAM into account, as explained elsewhere (8) (see Supporting Information Fig. S1 for ^{1}H-NMR spectra and Scheme S1 for the assignment of ^{1}H-NMR signals of PAMAM dendrimer).

Synthesis of *Cis*-Acontityl-Doxorubicin (CAD)

Cis-acontityl-doxorubicin (CAD) was synthesized using the method by Shen and Ryser (10) with modification. Briefly, *cis*-aconitic anhydride (27 mg, 173.1 μmol) in *p*-dioxane (1 ml) was added slowly to the aqueous solution of DOX (30 mg, 51.7 μmol in 10 ml distilled water) at room temperature with stirring, and the pH value was immediately adjusted to 8.5–8.7 with 0.5 M NaOH. After 10 min of reaction, the pH value was adjusted to 7.4, and the mixture was cooled to 4°C. The reaction mixture was further acidified to pH 2.5–3.0 by ice-cold 1 M HCl followed by ethyl acetate extraction (50 ml×2). The organic phase was then washed with saturated sodium chloride solution, dried with anhydrous sodium sulphate and evaporated under reduced pressure to yield a kind of bright red powder (14). The yield of CAD was 90.0%.

Analysis of CAD was carried out using a Shimadzu liquid chromatographic system (LC-10AT, Japan) with a UV detector (SPD-10A, Japan) operated at 490 nm. A Hypersil ODS C18 column (4.6×250 mm, 5 μm particle size) was used at 30°C. The mobile phase was $(NH_4)_2CO_3$ (3 *w*/*v*%) : methanol = 1 : 2 (*v*/*v*). The injection volume was 20 μl, and the flow rate was 1.0 ml/min. HPLC chromatogram of CAD (Fig. 1a) indicated that two products were obtained in the reaction (Rt = 5.05 min, CAD-1 and 5.60 min, CAD-2). Semi-preparative HPLCs were used to separate these two newly formed products, and both exhibited an identical mass value of 698.2 (M−H) by ESI mass spectrometry, which were in agreement with the literature (12), where the formation of two isomers of CAD were reported. As seen in Scheme 1, both CAD isomers possess the *cis*-carboxylic group necessary to catalyze the intramolecular hydrolysis of the amide bond (15), so we did not further separate them.

Synthesis of PEG-PAMAM-cis-aconityl-DOX Conjugates (PPCD Conjugates)

CAD was conjugated to the PEG-PAMAM conjugates in the presence of water-soluble carbodiimide EDC at room temperature in the dark (16). Briefly, CAD (45 mg, 60 mmol)

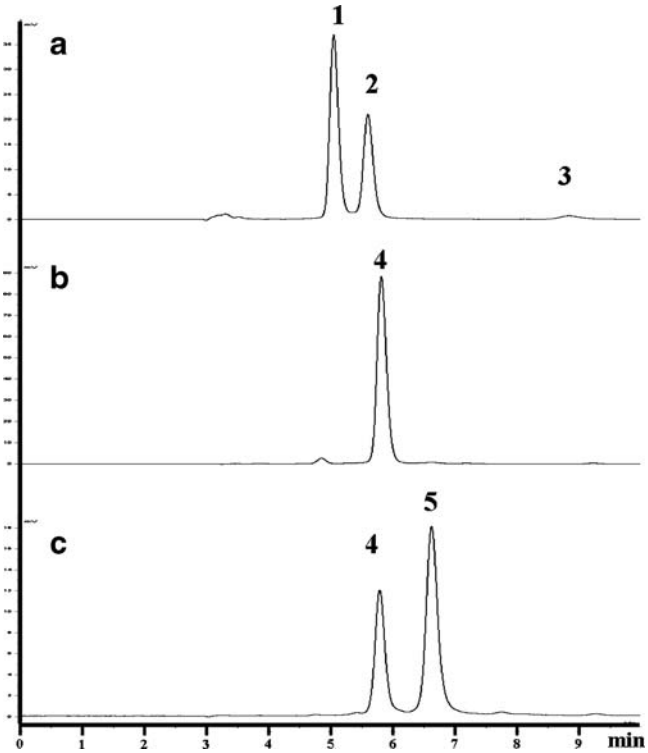

Fig. 1. HPLC chromatograms of CAD (**a**), reaction mixture of DOX and succinic anhydride after 3 h of reaction (**b**), and reaction mixture of SAD activation after 8 h of reaction (**c**). (1, CAD-1, Rt = 5.05 min; 2, CAD-2, Rt = 5.60 min; 3, DOX, Rt = 8.84 min; 4, SAD, Rt = 5.79 min; 5, SAD-NHS, Rt = 6.62 min).

and EDC (44 mg, 240 mmol) were dissolved in 10 ml of 0.1 M phosphate buffer (pH 6.0) and stirred at room temperature in the dark. After 30 min, PEG-PAMAM conjugate in 3 ml of distilled water (CAD: PEG-PAMAM = 48:1, molar ratio) was added, and pH value of the reaction mixture was adjusted to 8.0 by 0.5 M NaOH. The reaction mixture was then left to react in the dark for 12 h. Unreacted CAD and other small molecules were separated from the conjugate on a Sephadex G-25 fine column (3.6×55 cm) eluted with phosphate-buffered saline (pH 7.4). The macromolecular fractions of PPCD conjugates were collected, ultrafiltrated, dialyzed against distilled water and lyophilized to obtain red solids. The yields of PPCD 4/1, 16/1 and 32/1 were 68.4%, 71.0% and 71.6%, respectively.

Synthesis of PEG-PAMAM-succinic-DOX Conjugates (PPSD Conjugates)

As to the synthesis of PPSD, DOX was first converted to its succinic anhydride derivative (SAD) using the method reported by Luo *et al.* (17) with modification. DOX (25 mg, 43.1 μmol) was dissolved in anhydrous dimethylformamide (DMF) (1.65 ml), followed by addition of triethylamine (18.7 μl) and succinic anhydride (4.7 mg, 47.3 μmol). The reaction mixture was stirred at room temperature in the dark for 3 h. HPLC chromatogram of the reaction mixture showed the complete conversion of DOX (Rt = 8.84 min) to SAD (Rt = 5.79 min) (Fig. 1b). Then, 33.0 mg EDC (172.2 μmol) and 19.8 mg NHS (172.0 μmol) in 0.43 ml anhydrous DMF were added to the reaction mixture for another 8 h to form the active ester of SAD (SAD-NHS). The formation of SAD-NHS was confirmed by the appearance of a new peak with longer retention time (Rt = 6.62 min) in HPLC chromatogram (Fig. 1c). Although prolonged reaction time might produce more SAD-NHS, unknown peaks were detected in HPLC chromatogram, which might be due to the degradation of DOX under slightly alkaline condition. HPLC conditions were the same as those for CAD analysis.

PPSD conjugates were then prepared by coupling of PEG-PAMAM-NH_2 and SAD-NHS. The above reaction mixture containing SAD-NHS was added to PEG-PAMAM conjugate in phosphate buffer (pH 8.0) (SAD: PEG-PAMAM = 25:1, molar ratio), with the pH adjusted to 8.0 by 1 M HCl. After 12 h of reaction at room temperature, the reaction mixture was dialyzed against distilled water to remove DMF, and small molecular substances were separated from the conjugate on a Sephadex G-25 fine column (3.6×55 cm) eluted with PBS (pH 7.4). The macromolecular fractions of PPSD conjugates were collected, ultrafiltrated, dialyzed against distilled water and lyophilized to obtain red solids. The yields of PPSD 4/1, 16/1 and 32/1 were 75.4%, 77.6% and 82.6%, respectively.

Gel Permeation Chromatography (GPC)

GPC experiments were performed to evaluate the relative size of the synthesized conjugates. A Shimadzu liquid chromatographic system (LC-10AT, Japan) with a UV detector (SPD-10A, Japan) operated at 220 nm was used. A TSKgel G3000SWxl column (300×7.8 mm; 5 μm particle size) (Tosoh, Japan) was used at room temperature. The mobile phase was 0.01% triethylamine (*v*/*v*) aqueous solution with the flow rate of 0.5 ml/min, and the injection volume was 20 μl.

Dynamic Light Scattering (DLS) and Zeta Potential Measurement

The hydrodynamic diameters of G4 PAMAM dendrimer and the synthesized products, including PEG-PAMAM, PPCD and PPSD conjugates, were determined by dynamic light scattering using Zetasizer Nano ZS (Malvern Instruments Ltd., UK) (18). Samples were dissolved in 0.1 M PBS (pH 7.4, 10 mg/ml) and filtered through a Minisart High-Flow, PES 0.2 μm syringe filter (Sartorius Stedim Biotech GmbH, Germany) into the scattering cell. All measurements were carried out at 37°C. Zeta potential was determined using the same equipment. Samples were dissolved in 0.1× PBS (pH 7.4, 1 mg/ml) and all measurements were carried out at 37°C.

Determination of Total and Free Drug Content

Total drug content was quantified by hydrolyzing the glycosidic bond between the doxorubicinone and amino sugar at acidic condition and determining the released doxorubicinone (19). DOX-polymer conjugate (10 mg) was dissolved in distilled water (2 ml), 0.2 ml of the solution was mixed with 2.5 M HCl (0.8 ml) and methanol (1 ml), and the mixture was incubated at 50°C for 1.5 h to generate doxorubicinone, which was subsequently analyzed using a Shimadzu liquid chromatographic system (LC-10AT, Japan) with a UV detector (SPD-10A, Japan) operated at 490 nm. A Hypersil

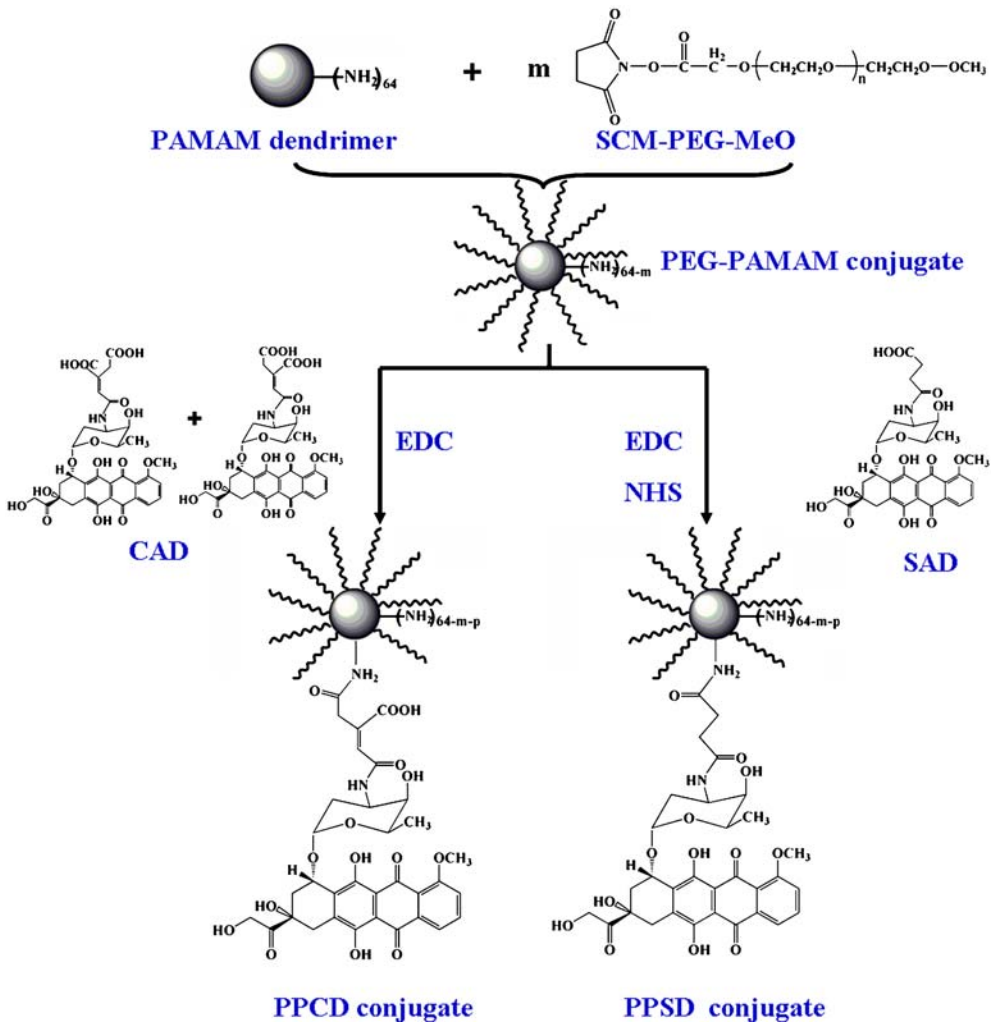

Scheme 1. Synthetic route for PPCD and PPSD conjugates.

ODS C18 column (4.6×250 mm, 5 μm particle size) was used at 30°C. The mobile phase was 0.01 M KH_2PO_4: acetonitrile: acetic acid = 45: 55: 0.27 (*v*/*v*/*v*). The injection volume was 20 μl, and the flow rate was 1.0 ml/min. A standard curve of doxorubicinone was generated by hydrolyzing free DOX at the same condition. Total drug content (wt.%) in each conjugate was calculated, and the conjugated number of DOX in each product was obtained.

The amount of free drug (unbound CAD or SAD) was determined by GPC method described above with minor modification (λ=490 nm). The free drug content was expressed as mol.% of the total drug, which was obtained from the relative area of peak corresponding to the free drug and that corresponding to the total drug (20).

In Vitro Release of DOX from Conjugates

DOX release from the conjugates was determined in pH 4.5, 5.5, 6.5 and 7.4 citrate buffer solutions (0.1 M) at 37°C. Dialysis bag (MWCO 3500) containing 1 ml of PPCD or PPSD conjugates (160 μg DOX-equiv.) citrate buffer solution was immersed in 40 ml of the buffer solution and incubated at 37°C. At fixed time intervals, sample was collected from outer fluid and subjected to HPLC analysis to obtain DOX release percentage. The HPLC condition was the same as the one used in determining total DOX content.

In Vitro Cytotoxicity Assay

SKOV-3 ovarian carcinoma cells were purchased from Institute of Biochemistry and Cell Biology (IBCB), Shanghai Institutes for Biological Sciences, Chinese Academy of Sciences (Shanghai, China) and cultured according to the previous report (21). The cytotoxicity of PAMAM dendrimer, PEG-PAMAM conjugates, free DOX and DOX-polymer conjugates against SKOV-3 cells was evaluated using MTT assay (22). The tested concentration ranges were 0–100 μM PAMAM-equiv. for PAMAM dendrimer and PEG-PAMAM conjugates, and 0–640 μM DOX-equiv for free DOX and DOX-polymer conjugates. The IC_{50} values were expressed as concentration (μM) of DOX-equiv. or PAMAM dendrimer-equiv.

Cellular Uptake

SKOV-3 cells were seeded on 35-mm glass-bottom culture dishes at a density of 1.25×10^5 cells/ml (2 ml cell suspension per well) and allowed to adhere for 24 h. DOX-polymer conjugates containing 32 μM DOX-equiv. in serum-

free culture media were added, and the cells were incubated for 60 min at 37°C. After incubation, conjugate solutions were removed, and the cells were washed three times with ice-cold PBS (pH 7.4). 0.5 ml of 0.25% trypsin-0.05% EDTA solution was added thereafter to detach the cells from the dishes (37°C, 4 min). Extracellular fluorescence was quenched by trypan blue (0.25% in 0.85% NaCl) for 5 min at room temperature (23). Finally, the cells resuspended in PBS were subjected to fluorescence-activated cell sorting (FACS) analysis. For the determination of total cellular fluorescence, the procedure of trypan blue quenching was omitted.

Cell-associated fluorescence was analyzed using a Becton Dickinson FACSCalibur cytometer (San Jose, CA, USA) equipped with an argon laser (488 nm) and emission filter for 550 nm. Data collection involved 10,000 counts per sample. The data were analyzed using CELLQuest™ software and expressed as the geometric mean of the entire population. Cells incubated without DOX-polymer conjugates were used to account for the background fluorescence.

Effects of Low Temperature and ATP Depletion on Cellular Uptake of DOX-polymer Conjugates

To evaluate the effect of low temperature on cellular uptake, SKOV-3 cells were pre-incubated at 4°C for 30 min. DOX-polymer conjugates (32 μM DOX-equiv.) were added thereafter at the same temperature for another 1 h. Cells were then washed and harvested for FACS analysis as described previously. Cellular uptake at 37°C was used as control. To evaluate the effect of ATP depletion, cells were pre-incubated with sodium azide (10 mM) and 2-deoxy-d-glucose (6.5 mM) in PBS (pH 7.4) at 37°C for 1 h (24). After pre-incubation, cells were treated with DOX-polymer conjugates (32 μM DOX-equiv.) in the presence of sodium azide and 2-deoxy-d-glucose at 37°C for another 1 h and were prepared for FACS analysis as described above.

Effect of Endocytosis Inhibitors on Cellular Uptake of DOX-polymer Conjugates

The cytotoxicity of sucrose, filipin, colchicine and poly-L-lysine (polylysine) against SKOV-3 cells was evaluated before inhibition study for the selection of nontoxic concentrations (see Supporting Information Fig. S5 for the selection of non-toxic concentrations). For the inhibition study, SKOV-3 cells were pre-incubated with 150 mg/ml of sucrose, 4 μg/ml of filipin, 40 μg/ml of colchicine and 800 μg/ml of polylysine for 30 min (sucrose 1 h) at 37°C. DOX-polymer conjugates containing 32 μM DOX-equiv. were added thereafter to co-incubate for another 1 h. Cells were washed and harvested for FACS analysis as described above.

Intracellular Localization of DOX-polymer Conjugates

SKOV-3 cells were grown on 35-mm glass-bottom culture dishes at a density of 2×10^4 cells/ml (2 ml of cell suspension per well) and were allowed to adhere for 24 h. DOX (1.7 μM), PPSD 32/1 and PPCD 32/1 (both 32 μM DOX-equiv.) (Ex 488 nm, Em 550 nm) in culture media were added, respectively. After 24 h of incubation, the drug-containing solutions were removed and 250 nM of Lysotracker Green DND-26 (Ex 504 nm, Em 511 nm) was added. Twenty minutes later, 5 μg/ml of Hoechst 33342 (Ex 345 nm, Em 478 nm) was added for another 10 min. After the staining solution was removed, cells were rinsed with PBS (pH 7.4) three times, fixed with 2% paraformaldehyde for 15 min at 4°C, and subjected to confocal laser scanning microscopy. Fluorescence images of cells were collected using a TCS SP2 confocal microscope (Leica, Heidelberg, Germany). In another group to study the effect of increased lysosomal pH on the intracellular fate of PPCD 32/1, 25 μM chloroquine was added to the culture dishes for 1 h at 37°C before the addition of PPCD 32/1.

In Vivo Fluorescence Imaging

In vivo fluorescence imaging analysis was used to evaluate the effect of PEGylation degree on the biodistribution of PPCD conjugates. Female BALB/c nu/nu mice, 5–6 weeks old (Shanghai SLAC Laboratory Animal Co., Ltd. Shanghai, China), were xenografted s.c. in the right flank with 5×10^6 SKOV-3 cells. When the tumors reached 0.4 to 0.6 cm in diameter, the tumor-bearing mice were subjected to *in vivo* imaging studies. PPCD 4/1, 16/1 and 32/1 dissolved in saline were injected into the tail vein of nude mice at a dose of 5 mg DOX-equiv./kg body weight. The same volume of saline was also injected as the control. The mice were anesthetized with i.p. administered 10% chloral hydrate; then, fluorescence images were obtained with the Maestro *In Vivo* imaging system (CRi, Woburn, MA, USA) at predetermined time points. Two filter sets (blue: excitation, 500–720 nm; exposure time, 300 ms and red: excitation, 670–900 nm; exposure time, 150 ms) were used to detect DOX-related fluorescence (from PPCD conjugates) and autofluorescence (primarily from the skin and blood vessels). The fluorescence images consisting of DOX-related fluorescence and autofluorescence spectra were then unmixed based on their spectral patterns using Maestro 2.6 software (CRi, Woburn, MA, USA).

To compare tissue and tumor distributions of PPCD conjugates, the mice were sacrificed at 48 h post-injection. Tumors and major organs, including livers, lungs, spleens, kidneys, and hearts, were dissected, washed with saline, and subjected to Maestro *In Vivo* imaging system to obtain both the real and fluorescence images. For *ex vivo* images, the background signal, due to the absence of autofluorescence produced by the skin and blood vessels, is not present; thus, a single-filter set (blue: excitation, 500–720 nm; exposure time, 300 ms) was used to detect DOX-related fluorescence. A quantification of *in vivo* distribution of the control and three PPCD conjugates was recorded as total photons per centimeter squared per steradian ($p/s/cm^2/sr$) per organ or tumor.

All animal experiments were carried out in accordance with guidelines evaluated and approved by the ethics committee of Fudan University (Shanghai, China).

Data Analysis

Results are presented as means ± standard deviations (SD) of three samples. Significant differences in the mean values were evaluated by Student's unpaired *t*-test. Places needing multiple comparisons were evaluated by one-way ANOVA with Boferroni correction. *P*-value of 0.05 or less was considered to be statistically significant.

RESULTS

Synthesis and Characterization of DOX-polymer Conjugates

The preparative scheme of PPCD and PPSD conjugates is shown in Scheme 1. Three PEG-PAMAM conjugates with different PEGylation degrees were synthesized by controlling the feed ratio of the starting materials. The PEGylation was confirmed by the appearance of signals at 3.2 ppm and 3.4–3.6 ppm in ^{1}H-NMR spectra of the conjugates, which correspond to the protons of CH_2CH_2O repeat unit and terminal OCH_3 groups of PEG, respectively. The conjugated numbers of PEG molecule were estimated to be 3.8, 12.9 and 20.1 when the feed molar ratio of PEG and PAMAM were 4:1, 16:1 and 32:1, respectively (Table I). DOX was then conjugated to the residual primary amino groups of PEG-PAMAM conjugates either by *cis*-aconityl or succinic linkage. By controlling the molar ratio of supplied CAD/SAD and PEG-PAMAM (48:1 and 25:1, respectively), we synthesized six DOX-polymer conjugates (see Supporting Information Fig. S2), each having about 14 DOX molecules grafted onto the surface of PEG-PAMAM conjugates (Table II). GPC was used to evaluate the purity of the products. As seen in Table II, unbound CAD/SAD was less than 0.6 mol.% of the total DOX content. Considering the fact that CAD/SAD was much less cytotoxic than the parent drug of DOX (data not shown), the effect of remaining CAD/SAD should be minimal.

The particle sizes of G4 PAMAM dendrimer, PEG-PAMAM and PPCD and PPSD conjugates were determined by dynamic light scattering. PEG-PAMAM conjugates showed increased particle size compared with unmodified PAMAM dendrimer (5.00±0.10 nm) ($P<0.05$), and coupling of DOX further increased the particle size of PEG-PAMAM 4/1, 16/1 and 32/1 by about 71–76 nm, 5.3–6.2 nm and 2.3–3.5 nm, respectively. These results were in agreement with findings from GPC experiments where shorter retention time indicated larger hydrodynamic volume (Tables I and II) (see Supporting Information Fig. S3 for size distribution maps and Fig. S4 for GPC chromatographs). All the PEGylated PAMAM dendrimers showed decreased zeta potential as compared with unmodified dendrimer (16.56±0.13 mV), and conjugation of DOX further decreased zeta potential (Tables I and II). PPCD conjugates seemed to be even less cationic than PPSD conjugates, as the newly introduced CAD molecule contains a carboxylic group which was able to ionize at netural pH condition.

In Vitro Release of DOX from Conjugates

According to the literature, macromolecules undergo a gradual pH decrease during endocytosis (25). The release profiles of DOX-polymer conjugates were investigated in the range of pH 4.5 to pH 7.4, which covered the pH condition from lysosome to plasma, respectively. As shown in Fig. 2, PPCD conjugates release DOX both time- and pH-dependently. All the PPCD conjugates released less than 5% of the total DOX over 96 h at pH 7.4 and 6.5. PPCD 32/1 released about 15.0% of DOX at pH 5.5. As pH further decreased to 4.5, accumulative release percentages of DOX from PPCD 32/1, 16/1 and 4/1 increased to 60.03±3.50%, 29.89±1.81% and 13.40±1.26%, respectively. In contrast to PPCD conjugates, PPSD conjugates released negligible amount of DOX (less than 1.0%) at any pH condition.

Cytotoxicity of DOX-polymer Conjugates Against SKOV-3 Cells

Fig. 3a shows the viability of SKOV-3 cells after 72 h of incubation with PAMAM dendrimer and PEG-PAMAM conjugates. G4 PAMAM dendrimer was indeed cytotoxic against SKOV-3 cells with the IC_{50} value of 1.13 μM. Modification by PEG reduced the cytotoxicity, showing an increased IC_{50} value (4.11 μM for PEG-PAMAM 4/1; IC_{50} value was not calculated for PEG-PAMAM 16/1 and 32/1 as more than 50% of cells were still alive even at the highest concentration). Results from Fig. 3a also indicated that higher PEGylation degree led to less cytotoxicity.

Fig. 3b and c show the viability of SKOV-3 cells after 72 h of incubation with DOX and DOX-polymer conjugates. The obtained IC_{50} value for free DOX against SKOV-3 cells was 0.23 μM, which was in the same magnitude with the result of a previous report (0.92 μM) (17). All the six DOX-polymer conjugates showed much lower cytotoxicity as compared with free DOX. PPCD 32/1 showed the highest cytotoxicity among the three PPCD conjugates with IC_{50} value of 27.83 μM, PPCD 16/1 (39.08 μM) and PPSD 32/1 (138.59 μM) ranking the second and third, respectively. IC_{50} values for the other three conjugates were not obtained, as more than 50% of cells were still alive even at the highest drug concentration.

Cellular Uptake

To differentiate between membrane-bound and internalized PPCD conjugates, trypan blue quenching assay was used to extinguish extracellular fluorescence (26). Fig. 4a displays the internalized and total fluorescence of SKOV-3 cells after incubation with DOX-polymer conjugates (32 μM DOX-equiv.). As depicted by the figure, total cellular fluorescence of six DOX-polymer conjugates did not display obvious tendency, while the internalized fluorescence decreased with increasing PEGylation degree. At the same PEGylation degree, the internalized fluorescence of PPSD conjugates

Table I. Characteristics of PEG-PAMAM Conjugates

Conjugates	Feed ratio PEG:PAMAM (by mole)	Number of conjugated PEG (by 1H NMR)	Particle size (nm)	GPC retention time(min)	Zeta potential (mv)
PEG-PAMAM 4/1	4:1	3.8	6.72±0.01	11.95	12.65±0.10
PEG-PAMAM 16/1	16:1	12.9	11.74±0.11	11.93	9.62±0.23
PEG-PAMAM 32/1	32:1	20.1	12.53±0.25	11.71	6.23±0.11

Table II. Characteristics of DOX-polymer Conjugates

Conjugates	DOX percentage (wt.%)	Unbound CAD/SAD[a] (mol.%)	Number of conjugated DOX	Particle size (nm) (n=3)	GPC retention time (min)	Zeta potential (mv) (n=3)
PPSD 4/1	18.18	0.26	14.0	77.92±2.96	10.69	10.12±0.05
PPSD 16/1	8.98	0.52	14.2	17.01±0.31	11.2	7.32±0.03
PPSD 32/1	6.18	0.35	13.7	14.78±0.95	11.25	5.23±0.07
PPCD 4/1	17.86	0.28	13.9	82.89±1.78	10.67	6.18±0.12
PPCD 16/1	8.53	0.14	13.5	17.90±0.33	11.18	4.00±0.03
PPCD 32/1	6.44	0.24	14.4	15.98±0.23	11.21	2.25±0.23

[a] CAD and SAD were the impurities for PPCD and PPSD conjugates, respectively.

was significantly greater than that of PPCD conjugates (P< 0.01). It seemed that the internalized percentage (internalized / total fluorescence) increased with increasing zeta potential of these conjugates (Fig. 4b), suggesting that the polycationic nature of PAMAM dendrimer played a positive role in the cellular uptake of the DOX-polymer conjugates.

Effects of Low Temperature and ATP Depletion on Cellular Uptake

In order to elucidate the internalization mechanism for the DOX-polymer conjugates, the effects of low temperature and ATP depletion on cellular uptake were evaluated in SKOV-3 cells. As seen in Fig. 5a, low temperature reduced the cellular uptake of PPCD 4/1, PPCD 16/1, PPCD 32/1, PPSD 4/1, PPSD 16/1 and PPSD 32/1 to 28.1%, 36.3%, 21.9%, 30.3%, 28.8% and 26.9% of the control, respectively. Pretreatment of sodium azide and 2-deoxy-d-glucose depleted cellular ATP, and decreased the cellular uptake of PPCD 4/1, PPCD 16/1, PPCD 32/1, PPSD 4/1, PPSD 16/1 and PPSD 32/1 to 50.7%, 47.9%, 58.8%, 58.0%, 67.0% and 55.6% of the control, respectively (Fig. 5b). All inhibitions were statistically significant (P<0.01). Inhibition of cellular uptake by low temperature and ATP depletion indicated that internalization of the DOX-polymer conjugates by SKOV-3 cells occurred through energy-dependent endocytosis.

Effects of Endocytosis Inhibitors on Cellular Uptake

Endocytosis, which occurs in most cells as pinocytosis, represents at least four basic mechanisms: clathrin-mediated endocytosis, caveolae-mediated endocytosis, macropinocytosis and clathrin- and caveolae-independent endocytosis (25). Clathrin-mediated endocytosis can be inhibited by a hyper-

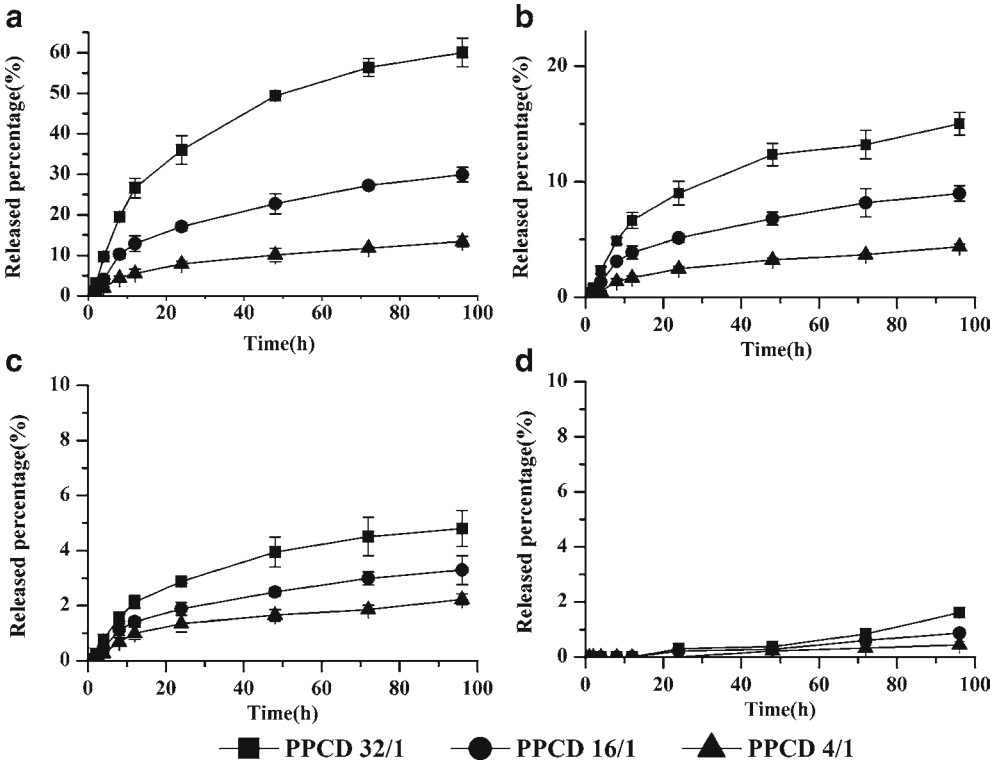

Fig. 2. *In vitro* release profiles of DOX from PPCD in citrate buffer solutions at pH 4.5 (**a**), 5.5 (**b**), 6.5 (**c**) and 7.4 (**d**). Data were expressed as mean ± standard deviation (n=3).

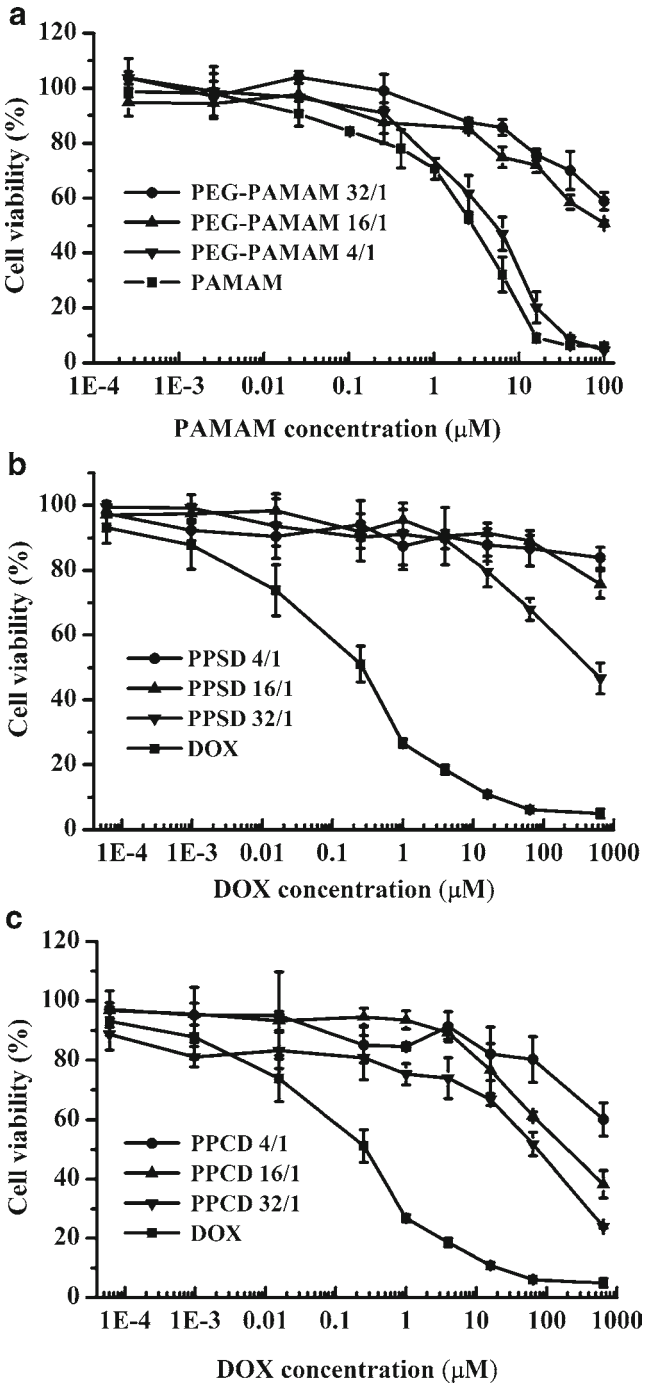

Fig. 3. *In vitro* cytotoxicity of PAMAM dendrimer, PEG-PAMAM conjugates, DOX and DOX-polymer conjugates against SKOV-3 cells after 72 h of incubation (**a**, PAMAM dendrimer and PEG-PAMAM conjugates; **b**, DOX and PPCD conjugates; **c**, DOX and PPSD conjugates). Data were expressed as mean ± standard deviation (n=3).

osmolar solution of sucrose, which blocks the formation of clathrin-coated pits (27). As shown in Fig. 6, sucrose decreased the cellular uptake of PPCD 4/1, PPCD 16/1, PPCD 32/1, PPSD 4/1, PPSD 16/1 and PPSD to 73.7%, 78.5%, 67.1%, 69.1%, 66.3% and 80.6% of the control, respectively (P<0.01) (Fig. 6), indicating the involvement of clathrin-mediated endocytosis in the cellular uptake of DOX-polymer conjugates.

Polylysine was reported to inhibit adsorption-mediated endocytosis by nonspecific interaction with negative charge in the cell surface (28). Incubation with polylysine reduced the cellular uptake of PPCD 4/1, PPCD 16/1, PPCD 32/1, PPSD 4/1, PPSD 16/1 and PPSD 32/1 to 70.4%, 69.9%, 83.5%, 61.5%, 75.0% and 79.3% of the control, respectively (P< 0.01), which showed the importance of surface positive charge on the internalization of PPCD and PPSD conjugates.

The effects of caveolae-mediated endocytosis and macropinocytosis on the internalization of the conjugates were evaluated using filipin, a caveolae-disrupting agent (29), and colchicines, a microtubule-disrupting agent (30), respectively. Neither of the two agents was found to influence the cellular uptake of six conjugates (P>0.05) (Fig. 6). These results suggested the minimal contribution of caveolae-mediated endocytosis and macropinocytosis.

Intracellular Localization of DOX-polymer Conjugates

The intracellular localization of free DOX, PPSD 32/1 and PPCD 32/1 conjugates in SKOV-3 cells was evaluated by

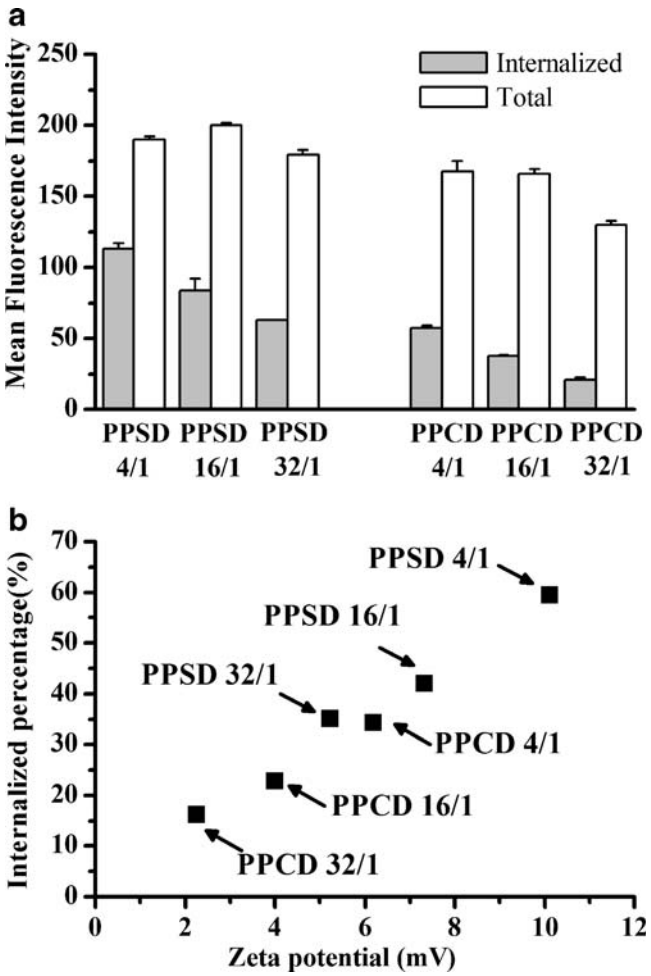

Fig. 4. **a** Internalized and total fluorescence of SKOV-3 cells after incubation with DOX-polymer conjugates (32 μM DOX-equiv.). Data were expressed as mean ± standard deviation (n=3). **b** Correlation between zeta potential of DOX-polymer conjugates and internalized percentage (Internalized percentage (%) = Internalized fluorescence / Total fluorescence × 100).

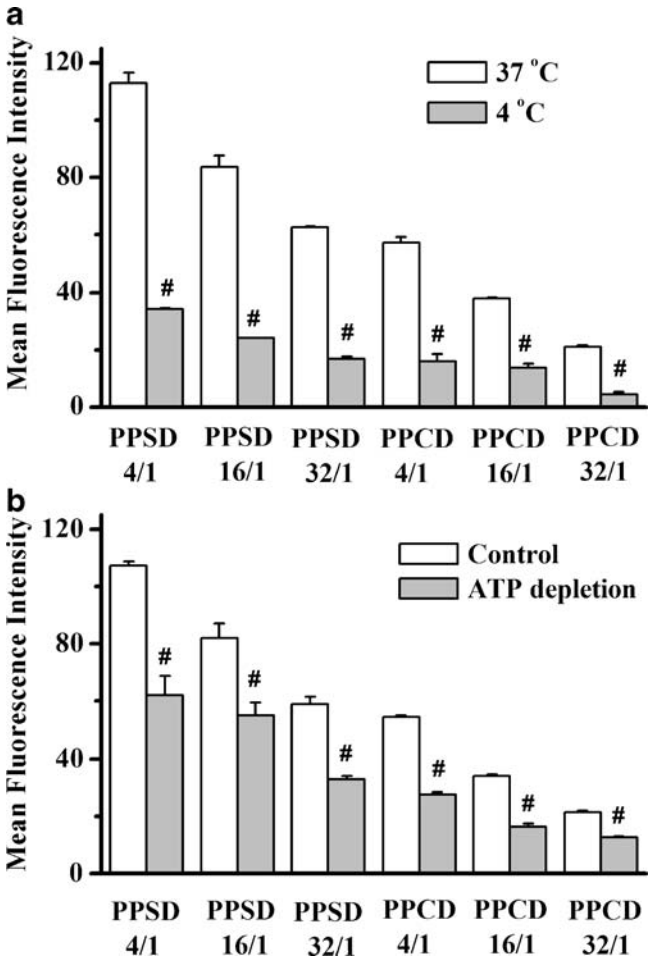

Fig. 5. Effects of low temperature (**a**) and ATP depletion (**b**) on cellular uptake of DOX-polymer conjugates. Data were expressed as mean ± standard deviation (n=3). # P<0.01, compared with each control.

confocal laser scanning microscopy. Free DOX was found to localize in the nuclei of SKOV-3 cells after 24 h incubation at 37°C, showing a co-localization with the blue fluorescence of Hoechst 33342 (Fig. 7a–d). PPSD 32/1 was found to localize in the acidic organelles (Fig. 7e–h), lysosomes and late endosomes as there is a clear co-localization with Lyso-Tracker green, a specific marker for these compartments, indicating that the conjugate taken up by the cells was delivered to lysosomes. No red fluorescence could be observed in the nuclei, indicating no DOX was released from the DOX-polymer conjugate by succinic linkage. As to PPCD 32/1, DOX-related fluorescence could be observed both in the lysosomes and nucleus, displaying clear co-localizaiton with LysoTracker green and Hoechst 33342 (Fig. 7i–l). The results suggested that PPCD 32/1 was able to release free DOX in the acidic organelles and into the nucleus. As expected, when the pH of the lysosomal compartment of SKOV-3 cells was enhanced by treatment with 25 μM chloroquine (31,32), no red fluorescence could be observed in the nuclei, indicating that DOX release from PPCD 32/1 was inhibited by enhanced lysosomal pH, and almost all the red fluorescence was localized in a perinuclear region of the cells after 24 h incubation at 37°C (Fig. 7m–p).

In Vivo Biodistribution of PPCD Conjugates

The time-dependent tumor accumulation of PPCD conjugates was determined non-invasively in SKOV-3 tumor-bearing nude mice, based on the fluorescence of DOX. Although commercial diet produced a strong fluorescence signal at the long wave fluorescence emission (600–700 nm) in the abdomen (33), other parts of the body, including the tumor sites, showed a minimal signal background when the mice were treated with saline. Therefore, the *in vivo* time-dependent biodistribution of PPCD conjugates could be visualized using *in vivo* optical imaging system. After intravenous injection, PPCD conjugates (5 mg DOX-equiv./kg) were found to accumulate in the tumor site in a time-dependent manner. The tumors could be delineated from the surrounding background tissue as early as 1 h after injection and exhibited a maximum fluorescence signal at 24 h post-injection with slight decrease at 48 h post-injection (Fig. 8a). The fluorescent intensity of the three conjugates in tumor sites increased with increasing PEGylation degree at any time point.

Ex vivo evaluation of excised tissues (liver, lung, spleen, kidney, and heart) and tumors at 48 h post-injection (Fig. 8b) showed an obvious tumor accumulation of these conjugates. As to the normal organs, liver and kidney showed obvious fluorescence, while limited accumulation was observed in heart, spleen and lung, indicating that all the conjugates were mainly taken up by tumor, liver and kidney. It could also be observed from the *ex vivo* fluorescence images that the tumor accumulation increased, and the accumulation in liver and kidney decreased with increasing the PEGylation degree. Quantification of the fluorescence intensity of these excised organs and tumors showed similar results to the above observation (Fig. 8c). The average fluorescence intensity of PPCD 32/1 in tumor was 2.21- and 1.69-fold higher than that of PPCD 4/1 and PPCD 16/1, respectively. In addition, liver accumulation of PPCD 32/1 was significantly decreased compared with PPCD 16/1 (P<0.01) and PPCD 4/1 (P< 0.01). Similar decreases were also observed in spleen and kidney.

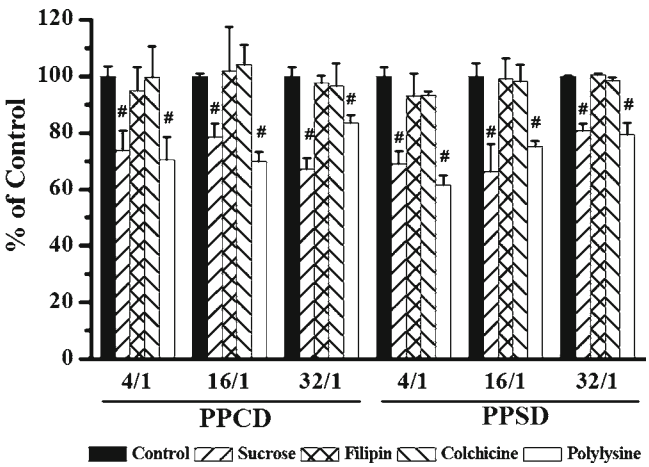

Fig. 6. Effects of endocytosis inhibitors on the cellular uptake of PPCD and PPSD conjugates. Data were expressed as mean ± standard deviation (n=3). # P<0.01, compared with each control.

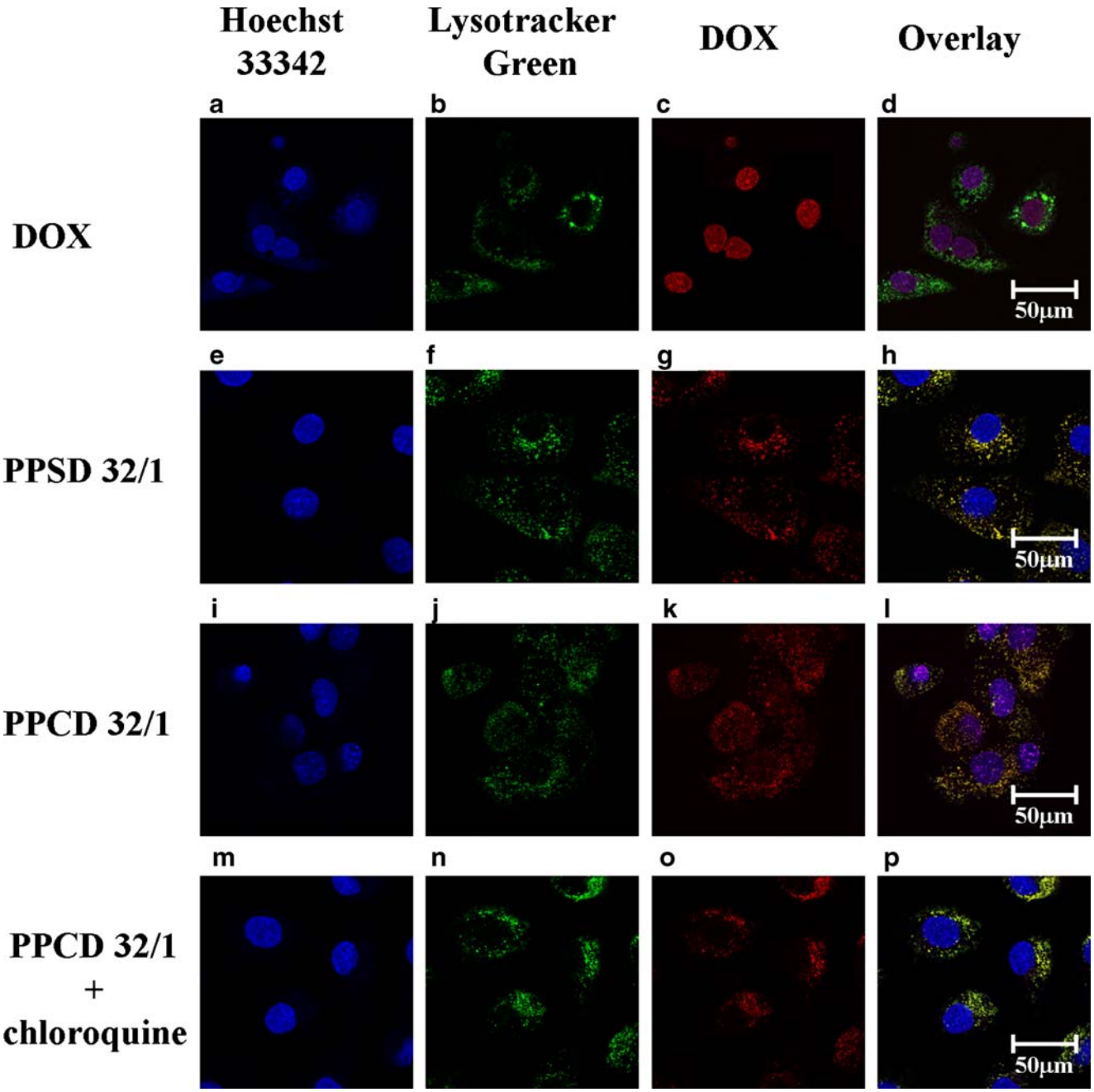

Fig. 7. Confocal laser scanning micrographs of SKOV-3 cells. SKOV-3 cell grown on glass-bottom culture dishes were incubated with DOX (1.7 μM) (**a**–**d**), PPSD 32/1 (32 μM DOX-equiv.) (**e**–**h**), and PPCD 32/1 (32 μM DOX-equiv.) (**i**–**l**) for 24 h, stained by Lysotracker Green (250 nM, 30 min) and Hoechst 33342 (5 μg/ml, 10 min) at 37°C, fixed by 2% PFA for 15 min at 4°C and observed by confocal laser scanning microscopy. Another group of cells was preincubated with 25 μM chloroquine for 1 h, incubated with PPCD 32/1 (32 μM DOX-equiv.) (**m**–**p**), stained and fixed following the same procedures, and observed by confocal laser scanning microscopy.

DISCUSSION

DOX is an effective anticancer agent and widely used in cancer therapy. However, its clinical use has been limited by dose-related side effects, such as cumulative cardiotoxicity, myelosuppression, nephrotoxicity, and extravasation (34). Therefore, it is necessary that DOX remain attached to the carrier during its transport in the bloodstream, but on arrival at the tumor site, the drug be liberated in an active form. The pH difference between the endosome/lysosome and the extracellular environment provides the advantage of using acid-sensitive linkage, which might be favorable in enhancing the antitumor effect of the drug while reducing possible side effects. In the present study, we synthesized six kinds of DOX-conjugated PEG-modified PAMAM dendrimers with three PEGylation degrees and two linkages for DOX conjugation, namely PPCD 4/1, PPCD 16/1, PPCD 32/1, PPSD 4/1, PPSD 16/1 and PPSD 32/1.

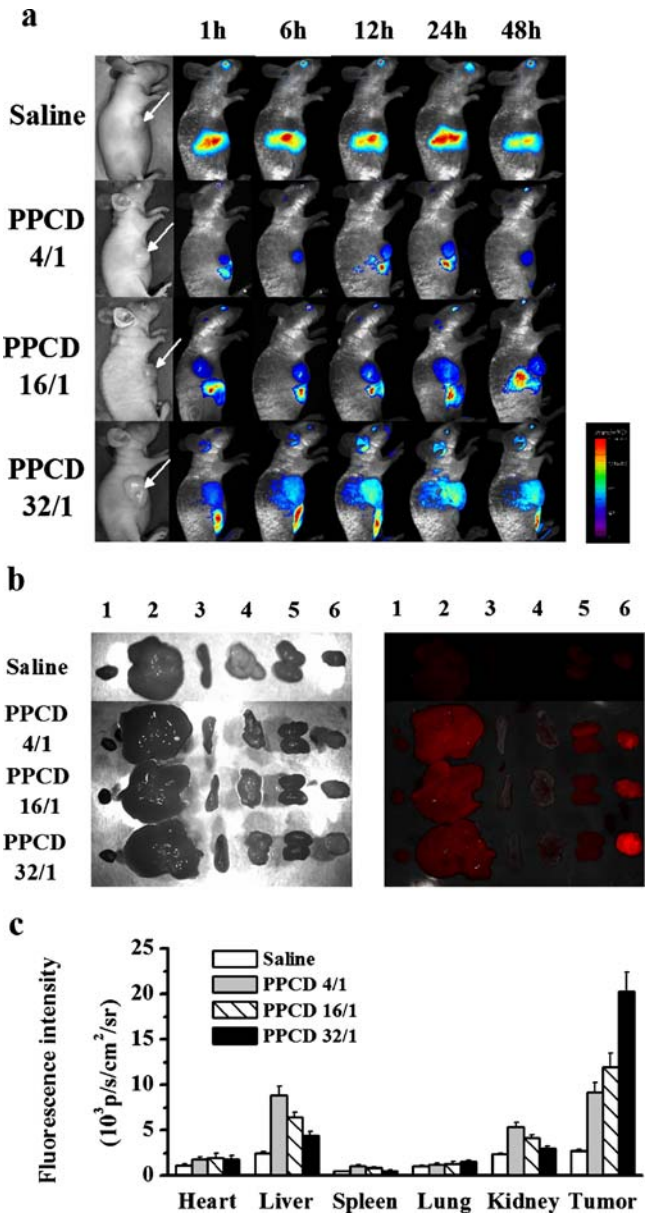

Fig. 8. **a** *In vivo* fluorescence imaging of subcutaneous SKOV-3 ovarian carcinoma tumor-bearing nude mice after intravenous injection of PPCD conjugates. *Arrow*, the position of the tumor. **b** Representative images of dissected organs of mice bearing SKOV-3 tumor sacrificed 48 h after intravenous injection of PPCD conjugates (*left*, real images; *right*, fluorescence images). *1*, heart; *2*, liver; *3*, spleen; *4*, lung; *5*, kidney; *6*, tumor. **c** Quantification of *in vivo* distribution of PPCD conjugates. Fluorescence intensity was recorded as photons per second per centimeter squared per steradian (*p/s/cm^2/sr*) per each excised organ at 48 h post-injection in SKOV-3 tumor-bearing mice (n=3).

PAMAM dendrimer was first modified with different numbers of PEG molecules to produce conjugates with different PEGylation degrees. Both GPC and DLS results showed that the size of PEG-PAMAM conjugates increased after PEGylation. According to the literature (35), grafted PEG chains assume mushroom or brush conformation depending on PEG concentration at the surface of nanocarriers. In the case of low PEGylation degree, PEG chains are folded around the anchoring site into a compact structure, which is the mushroom conformation, while at higher PEGylation degree, neighboring PEG chains push against each other, and as a result, extend further out from the surface, leading to the brush conformation. It is possible that PEG grafted on the surface of PAMAM dendrimer undergoes mushroom-brush transition in its conformation when the conjugated number of PEG molecule increases from 3.8 to 20.1, thus resulting in growing hydrodynamic volume.

Conjugation of DOX to PEG-PAMAM conjugates further increased the particle size. It is possible that DOX molecules insert into the interval of PEG chains and lead to larger hydrodynamic diameters by steric repulsion. Similar results observed by Sadzuka *et al.* (35) found that insertion of short chain PEG-lipid into the interval of a large one led to the enlargement of mushroom configuration. However, the increments in hydrodynamic diameter varied widely among PEG-PAMAM conjugates with different PEGylation degrees. Dramatic size increase was observed in PEG-PAMAM 4/1 after DOX conjugation. It has been reported that enough repulsion (electrostatic or steric) between individual particles was necessary to prevent particles from aggregation (36). DOX coupling consumed primary amine groups and reduced the electrostatic repulsion between PEG-PAMAM conjugates. At the same time, possible hydrophobic interaction among the monomers of DOX-polymer conjugates was introduced. Therefore, it is possible that in the case of low PEGylation degree, steric repulsion produced by PEG chains may not be strong enough to keep the DOX-polymer from aggregating, and aggregates can be formed. While at higher PEGylation degree, DOX-polymer conjugates exhibited relatively small hydrodynamic diameters of about 14–18 nm (Table II), which were similar to the diameters of their respective PEG-PAMAM conjugates (11–13 nm, Table I). These results suggest that PPCD 16/1, PPCD 32/1, PPSD 16/1 and PPSD 32/1 do not aggregate in aqueous solution and probably exist as monomers. It was also found that PEG-PAMAM 16/1 exhibited larger hydrodynamic diameters than PEG-PAMAM 32/1 after DOX conjugation. Possible explanations were that the particle size of monomer was determined by both the PEGylation degree and surface charge. It is possible that synthesis of PPCD 32/1 and PPSD 32/1 consume too much primary amine groups, and repulsion between the dendrimer arms decreases significantly, leading to the shrinkage of the dendrimer structure and reduced hydrodynamic diameter. It has been reported from the literature (37) that the size of the acetylated G5 PAMAM dendrimers is smaller than unmodified G5 PAMAM dendrimer because acetylation consumed surface primary amine groups, reduced the electrostatic repulsion between dendrimer arms and subsequently resulted in a less extended conformation than the unmodified dendrimer.

PPSD conjugates with DOX conjugated via amide bond were quite stable and released negligible DOX under either neutral or mildly acidic conditions. As expected, PPCD conjugates released DOX in a pH-dependent manner. It seemed that the acid-triggered release of DOX from PPCD conjugates increased with increasing PEGylation degree. The reason might be that the released DOX molecules were potentially encapsulated into the hydrophobic core of PAMAM dendrimer due to the difference in solubility. The

alkyl chains in the structure of PAMAM dendrimer provide a hydrophobic condition to incorporate hydrophobic drugs, including DOX (38,39). The increased PEGylation degree might enhance the relative solubility of DOX in the bulk solution, decrease the encapsulated DOX amount and lead to the greater release. As a matter of fact, in our experiments 14 DOX molecules seemed to be the maximum number that can be conjugated to PEG-PAMAM 4/1. Further increasing the feed ratio of CAD and PEG-PAMAM 4/1 led to the formation of insoluble substances. However, more DOX molecules could be attached to PEG-PAMAM 16/1 and 32/1 (data not shown). These results suggested the greater solubilizing effect of PAMAM dendrimer with higher PEGylation degree.

Much of the literature has investigated the cellular internalization mechanism of PAMAM dendrimers. The obtained results seemed to be dependent on the cell models utilized and also the surface modification. Kitchens *et al.* (40,41) reported that uptake of cationic (G2 and G4) PAMAM dendrimers into Caco-2 cells was via clathrin-dependent endocytosis, whereas G4 PAMAM dendrimer was predominately internalized via a cholesterol-dependent route in B16F10 melanoma cells (42). More recently, Saovapakhiran *et al.* (43) found that G3 PAMAM dendrimer was internalized by HT-29 cells via both caveolae-dependent and macropinocytosis pathways. In the same experiments (43), endocytosis pathways remained unchanged when the dendrimer was modified with two propranolol molecules (G3P2). However, when it was modified with two lauroyl chains (G3L2), the dendrimer conjugate was internalized via clathrin-dependent, caveolae-dependent, and macropinocytosis pathways, and the internalization of G3L2P2 dendrimer conjugate appears to involve a caveolae-dependent endocytosis pathway. In the present study, endocytosis inhibition experiments have demonstrated that PPCD and PPSD conjugates were internalized by SKOV-3 cells via clathrin-mediated endocytosis, while the contribution of caveolae-mediated endocytosis and macropinocytosis was minimal.

Macromolecules undergo different extents of pH decrease when internalized via different endocytic pathways. During clathrin-mediated endocytosis, the pH value of the internalized vesicles drops gradually from 7.4 in the culturing media to 6.2–6.5 in the early endosomes, 5.5 in late endosomes and finally to as low as 4.5 in the lysosomes (25). However, caveolae-mediated endocytosis delivers macromolecules to non-lysosomal compartments, and the pH of formed caveosomes is neutral (44). As to macropinocytosis, although the formed macropinosomes decrease their pH, they do not fuse with lysosomes (45), and thus may not be as acidic as the lysosomes. The results of *in vitro* release experiments had demonstrated that DOX release at pH 5.5 was dramatically reduced to about 25–33% of that at pH 4.5, so the difference in endocytic pathway might significantly affect the acid-sensitive release of DOX from PPCD conjugates. Endocytosis inhibition experiments have demonstrated that DOX-polymer conjugates were internalized by SKOV-3 cells via clathrin-mediated endocytosis, which, in contrast with caveolae-mediated endocytosis and macropinocytosis, delivered the conjugates to the lysosomes, triggered the acid-sensitive release of DOX from PPCD conjugates and enabled the entrance of DOX into the nuclei to exert its cell-killing effect. The lysosome-directed drug delivery was further confirmed by confocal laser scanning microscopy. The full co-localization of PPCD conjugates and Lysotracker Green, the specific marker for late endosomes and lysosomes, provided convincing evidence. The acid-sensitive release of DOX from PPCD conjugates was also confirmed by the co-localization of DOX and Hoechst 33342 in the nucleus of SKOV-3 cells. Inhibition of DOX release by chloroquine, a lysosomal pH-enhancing agent, also provided strong evidence that acidic condition was essential for the efficient drug release and therefore the antitumor effect.

We further used *in vivo* fluorescence imaging analysis to evaluate the effect of PEGylation degree on the biodistribution of PPCD conjugates. As expected, PPCD 32/1 behaved the most favorably in terms of *in vivo* distribution profile. Its tumor accumulation was the most, and the uptake by liver and spleen were the least among the three evaluated conjugates. The reasons might be due to the highest PEGylation degree. According to the literature (46), grafted PEG chains create a barrier layer to block the adhesion of opsonins present in the blood serum so that the particles can remain camouflaged or invisible to phagocytic cells and exhibit less accumulation in RES (liver and spleen).

Taking into account the results of *in vitro* release, cellular uptake, cytotoxicity and intracellular localization, we could find that acid-sensitive DOX release and lysosomal delivery of the conjugates played an important role in determining the cytotoxicity of PPCD conjugates. In other words, internalized PPCD conjugates were delivered to lysosomes where the slightly acidic condition permitted the release of DOX and the subsequent entrance into nucleus to exert its cytotoxicity. This is indeed explainable as DOX has been reported to cause cell cycle arrest by initiation of DNA damage through several proposed mechanisms that require the presence of drug in the nucleus and direct interaction with genomic DNA (47). Malugin *et al.* (48) also found that DOX release from HPMA copolymer conjugate was essential for the induction of cell cycle arrest and the formation of nuclear fragmentation and apoptotic body. On the other hand, DOX was also reported to damage cells by producing hydrogen peroxide (49). Therefore, the possibility could not be excluded that DOX might exert its anticancer effect as early as in the cytoplasm. The fact that the cytotoxicity of PPCD conjugates increased with increasing PEGylation degree also suggested the importance of release extent of DOX.

CONCLUSION

Using PEGylated PAMAM denderimers as the backbone, we synthesized and characterized a series of DOX-polymer conjugates with different PEGyaltion degrees and drug conjugation styles: PPSD 4/1, PPSD 16/1, PPSD 32/1, PPCD 4/1, PPCD 16/1 and PPCD 32/1. Both PEGylation degree and drug conjugation style were found to affect the *in vitro* release, *in vitro* cytotoxicity and cellular uptake. The acid-sensitive DOX release was the determinant of the *in vitro* cytotoxicity against SKOV-3 cells. Mechanistic studies revealed that the DOX-polymer conjugates were internalized by SKOV-3 cells via clathrin-mediated endocytosis, which ensured their localization in the acidic cellular compartments, subsequent release of DOX from PPCD conjugates and final

entrance into the nucleus. *In vivo* fluorescence imaging analysis demonstrated that PPCD 32/1 accumulated in tumor site most efficiently. Considering its most efficient acid-sensitive drug release and nuclear accumulation, which might lead to highest cytotoxicity, and highest PEGylation degree, which might result in most favorable *in vivo* behavior, PPCD 32/1 might be a potential candidate for solid tumor treatment and worthy of further investigation.

ACKNOWLEDGEMENTS

This work was supported by the National Basic Research Program of China (973 Program) 2007CB935802, National Natural Science Foundation of China (30672543) and National Key Program Pharmaceutical Innovation and Development (2009ZX09310-006).

REFERENCES

1. Khandare J, Minko T. Polymer–drug conjugates: progress in polymeric prodrugs. Prog Polym Sci. 2006;31:359–97.
2. Patri AK, Majoros I, Baker JR Jr. Dendritic polymer macromolecular carriers for drug delivery. Curr Opin Chem Biol. 2002;6:466–71.
3. Moghimi SM, Hunter AC, Murry JC. Nanomedicine: current status and future prospects. FASEB J. 2005;19:311–30.
4. Majoros IJ, Thomas TP, Mehta CB, Baker JR Jr. Poly(amidoamine) dendrimer-based multifunctional engineered nanodevice for cancer therapy. J Med Chem. 2005;48:5892–9.
5. Patri AK, Myc A, Beals J, Thomas TP, Bander NH, Baker JR Jr. Synthesis and *in vitro* testing of J591 antibody–dendrimer conjugates for targeted prostate cancer therapy. Bioconjugate Chem. 2004;15:1174–81.
6. Malik N, Wiwattanapatapee R, Klopsch R, Lorenz K, Frey H, Weener JW. Dendrimers: relationship between structure and biocompatibility *in vitro*, and preliminary studies on the biodistribution of 125I-labeled polyamidoamine dendrimers *in vivo*. J Control Release. 2000;65:133–48.
7. Calabretta MK, Kumar A, McDermott AM, Cai C. Antibacterial activities of poly(amidoamine) dendrimers terminated with amino and poly(ethylene glycol) groups. Biomacromolecules. 2007;8: 1807–11.
8. Luo D, Haverstick K, Belcheva N, Han E, Saltzman WM. Poly (ethylene glycol)-conjugated PAMAM dendrimer for biocompatible, high-efficiency DNA delivery. Macromolecules. 2002;35: 3456–62.
9. Kratz F, Beyer U, Schutte MT. Drug-polymer conjugates containing acid-cleavable bonds. Crit Rev Ther Drug Carrier Syst. 1999;16: 245–88.
10. Shen WT, Ryser HJP. Cis-aconityl spacer between daunomycin and macromolecular carriers: a model of pH-sensitive linkage releasing drug from a lysosomotropic conjugate. Biochem Biophys Res Commun. 1981;102:1048–54.
11. Ulbrich K, Etrych T, Chytil P, Jelínková M, Ríhová B. HPMA copolymers with pH-controlled release of doxorubicin: *in vitro* cytotoxicity and *in vivo* antitumor activity. J Control Release. 2003;87:33–47.
12. Kakinoki A, Kaneo Y, Ikeda Y, Tanaka T, Fujita K. Synthesis of poly(vinyl alcohol)-doxorubicin conjugates containing cis-aconityl acid-cleavable bond and its isomer dependent doxorubicin release. Biol Pharm Bull. 2008;31:103–10.
13. Yoo HS, Lee EA, Park TG. Doxorubicin-conjugated biodegradable polymeric micelles having acid-cleavable linkages. J Control Release. 2002;82:17–27.
14. Zhu Z, Kralovec J, Ghose T, Mammen M. Inhibition of Epstein-Barr-virus-transformed human chronic lymphocytic leukaemic B cells with monoclonal-antibody-Adriamycin (doxorubicin) conjugates. Cancer Immunol Immunother. 1995;40:257–67.
15. Bender ML. General acid-base catalysis in the intramolecular hydrolysis of phthalamic acid. J Am Chem Soc. 1957;79:1258–9.
16. Hudecz F, Ross H, Price MR, Baldwin RW. Immunoconjugate design: a predictive approach for coupling of daunomycin to monoclonal antibodies. Bioconjugate Chem. 1990;1:197–204.
17. Luo Y, Bernshaw NJ, Lu ZR, Kopecek J, Prestwich GD. Targeted delivery of doxorubicin by HPMA copolymer-hyaluronan bioconjugates. Pharm Res. 2002;19:396–402.
18. Saovapakhiran A, D'Emanuele A, Attwood D, Penny J. Surface modification of PAMAM dendrimers modulates the mechanism of cellular internalization. Bioconjugate Chem. 2009;20:693–701.
19. Tomlinson R, Heller J, Brocchini S, Duncan R. Polyacetal-doxorubicin conjugates designed for pH-dependent degradation. Bioconjugate Chem. 2003;14:1096–106.
20. Chytil P, Etrych T, Konák C, Sírová M, Mrkvan T, Boucek J. New HPMA copolymer-based drug carriers with covalently bound hydrophobic substituents for solid tumour targeting. J Control Release. 2008;127:121–30.
21. Yoshimoto M, Ogawa K, Washiyama K, Shikano N, Mori H, Amano R. Alpha(v)beta(3) integrin-targeting radionuclide therapy and imaging with monomeric RGD peptide. Int J Cancer. 2008;123:709–15.
22. Greco F, Vicent MJ, Gee S, Jones AT, Gee J, Nicholson RI. Investigating the mechanism of enhanced cytotoxicity of HPMA copolymer-Dox-AGM in breast cancer cells. J Control Release. 2007;117:28–39.
23. Raucher D, Chilkoti A. Enhanced uptake of a thermally responsive polypeptide by tumor cells in response to its hyperthermia-mediated phase transition. Cancer Res. 2001;61:7163–70.
24. Massodi I, Bidwell GL III, Raucher D. Evaluation of cell penetrating peptides fused to elastin-like polypeptide for drug delivery. J Control Release. 2005;108:396–408.
25. Liu J, Shapiro JI. Endocytosis and signal transduction: basic science update. Biol Res Nurs. 2003;5:117–28.
26. Hed J, Hallden G, Johansson SG, Larsson P. The use of fluorescence quenching in flow cytofluorometry to measure the attachment and ingestion phases in phagocytosis in peripheral blood without prior cell separation. J Immunol Methods. 1987;101:119–25.
27. Heuser JE, Anderson RG. Hypertonic media inhibit receptor-mediated endocytosis by blocking clathrin-coated pit formation. J Cell Biol. 1989;108:389–400.
28. Lu W, Sun Q, Wan J, She Z, Jiang XG. Cationic albumin-conjugated pegylated nanoparticles allow gene delivery into brain tumors via intravenous administration. Cancer Res. 2006; 66:11878–87.
29. Schnitzer JE, Oh P, Pinney E, Allard J. Filipin-sensitive caveolar-mediated transport in endothelium: reduced transcytosis, scavenger endocytosis, and capillary permeability of selected macromolecules. J Cell Biol. 1994;127:1217–32.
30. Kansara V, Paturi D, Luo S, Gaudana R, Mitra AK. Folic acid transport via high affinity carrier-mediated system in human retinoblastoma cells. Int J Pharm. 2008;355:210–9.
31. Krogstad DJ, Schlesinger PH. The basis of antimalarial action: non-weak base effects of chloroquine on acid vesicle pH. Am J Trop Med Hyg. 1987;36:213–20.
32. Yang HM, Reisfeld RA. Doxorubicin conjugated with a monoclonal antibody directed to a human melanoma-associated proteoglycan suppresses the growth of established tumor xenografts in nude mice. Proc Natl Acad Sci U S A. 1988;85: 1189–93.
33. Lee SJ, Park K, Oh YK, Kwon SH, Her S, Kim IS. Tumor specificity and therapeutic efficacy of photosensitizer-encapsulated glycol chitosan-based nanoparticles in tumor-bearing mice. Biomaterials. 2009;30:2929–39.
34. Blum RH, Carter SH. Adriamycin: a new anticancer drug with significant clinical activity. Ann Intern Med. 1974;80:249–59.
35. Sadzuka Y, Nakade A, Hirama R, Miyagishima A, Nozawa Y, Hirota S. Effects of mixed polyethyleneglycol modification on fixed aqueous layer thickness and antitumor activity of doxorubicin containing liposome. Int J Pharm. 2002;238:171–80.
36. Glodde M, Sirsi SR, Lutz GJ. Physiochemical properties of low and high molecular weight poly(ethylene glycol)-grafted poly

(ethylene imine) copolymers and their complexes with oligonucleotides. Biomacromolecules. 2006;7:347–56.
37. Majoros IJ, Keszler B, Woehler S, Bull T, Baker JR Jr. Acetylation of poly(amidoamine) dendrimers. Macromolecules. 2003;36:5526–9.
38. Papagiannaros A, Dimas K, Papaioannou GT, Demetzos C. Doxorubicin-PAMAM dendrimer complex attached to liposomes: cytotoxic studies against human cancer cell lines. Int J Pharm. 2005;302:29–38.
39. Ke W, Zhao Y, Huang R, Jiang C, Pei Y. Enhanced oral bioavailability of doxorubicin in a dendrimer drug delivery system. J Pharm Sci. 2008;97:2208–16.
40. Kitchens KM, Foraker AB, Kolhatkar RB, Swaan PW, Ghandehari H. Endocytosis and interaction of poly (amidoamine) dendrimers with Caco-2 cells. Pharm Res. 2007;24:2138–45.
41. Kitchens KM, Kolhatkar RB, Swaan PW, Ghandehari H. Endocytosis inhibitors prevent poly(amidoamine) dendrimer internalization and permeability across Caco-2 cells. Mol Pharm. 2008;5:364–9.
42. Seib FP, Jones AT, Duncan R. Comparison of the endocytic properties of linear and branched PEIs, and cationic PAMAM dendrimers in B16f10 melanoma cells. J Control Release. 2007;117:291–300.
43. Saovapakhiran A, D'Emanuele A, Attwood D, Penny J. Surface modification of PAMAM dendrimers modulates the mechanism of cellular internalization. Bioconjugate Chem. 2009;20:693–701.
44. Pelkmans L, Kartenbeck J, Helenius A. Caveolar endocytosis of simian virus 40 reveals a new two-step vesicular-transport pathway to the ER. Nat Cell Biol. 2001;3:473–83.
45. Hamasaki M, Araki N, Hatae T. Association of early endosomal autoantigen 1 with macropinocytosis in EGF-stimulated A431 cells. Anat Rec A Discov Mol Cell Evol Biol. 2004;277:298–306.
46. Owens DE III, Peppas NA. Opsonization, biodistribution, and pharmacokinetics of polymeric nanoparticles. Int J Pharm. 2006;307:93–102.
47. Gewirtz DA. A critical evaluation of the mechanisms of action proposed for the antitumor effects of the anthracycline antibiotics adriamycin and daunorubicin. Biochem Pharmacol. 1999;57:727–34.
48. Malugin A, Kopecková P, Kopecek J. Liberation of doxorubicin from HPMA copolymer conjugate is essential for the induction of cell cycle arrest and nuclear fragmentation in ovarian carcinoma cells. J Control Release. 2007;124:6–10.
49. Mizutani H, Tada-Oikawa S, Hiraku Y, Kojima M, Kawanishi S. Mechanism of apoptosis induced by doxorubicin through the generation of hydrogen peroxide. Life Sci. 2005;76:1439–53.